Monitoring autumn agriculture activities using Synthetic Aperture Radar (SAR) and coherence change detection

Laura Dingle Robertson [a,1,*], Heather McNairn [a], Marco van der Kooij [b], Xianfeng Jiao [a], Samuel Ihuoma [a], Pamela Joosse [c]

[a] *Agriculture and Agri-food Canada, Agri-Environment Division, Ottawa, Ontario, Canada*
[b] *Vanderkooij Consult, Ottawa, Ontario, Canada*
[c] *Agriculture and Agri-food Canada, Harrow Research & Development Centre, Harrow, Ontario, Canada*

ARTICLE INFO

ABSTRACT

Across Canada, farmers are encouraged to adopt beneficial management practices (BMPs) to protect soil heath, reduce green house gas emissions and mitigate off-site impacts from agriculture. Measuring the uptake of BMPs, including the implementation of conservation tillage, helps gauge the success of policies and programs to promote adoption. Satellites are one way to monitor BMP adoption and Synthetic Aperture Radars (SARs) are of particular interest given their all-weather data collection capability. This research investigated coherent change detection (CCD) to determine when farmers harvest and till their fields. A time series of both Sentinel-1 and RADARSAT Constellation Mission (RCM) images was acquired over a site in the Canadian Lake Erie basin, during the autumn of 2021, when farmers were harvesting and tilling fields of corn, soybeans and wheat. 16 CCD pairs were created and coherence values were interpreted based on observations collected for 101 fields. An m-chi decomposition was applied to the RCM data, and the Volume/Surface (V/S) ratio was calculated as an additional source of information to interpret results. Change events due to harvest, tillage, autumn seeding and chemical termination resulted in coherence values below 0.20. The mean and standard deviation for fields with observed change was 0.18 ± 0.03. Coherence values were 0.42 ± 0.15 for fields where no change was noted. Tests confirmed that the coherence associated with changed and unchanged fields was significantly different. Coherence values could also differentiate between some types of management events, including tillage and harvest. CCD could also separate harvest as a function of crop type (corn or soybeans). V/S ratios declined after tillage events but increased after both harvesting and chemical termination. Narrowing the date of harvest and tillage is as important as detecting change. To meet this requirement, Sentinel-1 and RCM CCD products with values below 0.20 (indicating change had occurred), were graphically overlaid. With this approach, the timing of corn harvest was identified as occurring within a 5-day window. The tilling of corn, soybeans and wheat was narrowed to a 4-day window. The results of this research confirmed that CCD can be used to capture change due to autumn agricultural activities, and this technique can also separate change due to harvest and tillage. Finally, this study demonstrated that when data from different SAR missions are combined in a virtual constellation, timing of harvest and tillage can be more precisely defined.

* Corresponding author.
  E-mail address: laura.dingle-robertson@ec.gc.ca (L. Dingle Robertson).
[1] Present address & affiliation, Environment and Climate Change Canada, Landscape Science and Technology Division, Ottawa, Ontario, Canada.

1. Introduction

Conventional tillage activities, such as moldboard plowing and multiple tillage passes, have negative effects on both soil and water ecosystems [1,2]. These types of practices can increase water and wind erosion, increase greenhouse gas emissions, and negatively affect soil biodiversity [1–4]. Reducing the number of tillage passes, using conservation tillage implements, delaying tillage until just prior to seeding or directly seeding into untilled soils, will reduce erosion risk and promote good soil health [1,2]. With these agriculture best management practices (BMPs), producers can maintain productivity while lessening the impacts of agriculture on the soil and surrounding ecosystems [5].

Reducing soil disturbance, by using conservation tillage implements or limiting the number of tillage passes, can mitigate runoff of nutrients and pesticides into aquatic systems. Adoption of these BMPs is being encouraged in the Great Lakes basin. Lake Erie is the smallest of the five Great Lakes by volume of water, yet this lake provides drinking water to 12.5 million people in both Canada and the United States [6]. The water quality of Lake Erie is impacted by both point source pollution and non-point runoff from intensive agricultural production in the basin [7]. Excess phosphorus loadings are of particular concern, with the majority of the non-point source contributions originating from agricultural lands [7]. Both Canadian federal and provincial governments have invested significant funds (over $15 million CDN since 2018) to encourage farmers to improve soil health and water quality in this region, including equipment modifications to reduce tillage [8]. With these efforts to promote adoption, an approach is required to measure the uptake of conservation tillage to gauge the outcome of policies and programs to promote these BMPs. This programmatic need to monitor reduced tillage for this important Canadian watershed is the motivation for the research presented in this manuscript.

1.1. Monitoring tillage using Synthetic Aperture Radar (SAR)

Earth observation satellites acquire images over large geographies and could provide data to identify if and when fields are tilled. The revisit period of satellites varies, but these platforms typically provide a re-look at agriculture fields with periods between image acquisitions ranging from days to weeks. Satellites are able to repeatedly capture changes in field conditions throughout the busy harvesting and seeding periods [9–12].

Synthetic Aperture Radar (SAR) sensors transmit pulses of energy at microwave frequencies. An important advantage associated with SARs is the ability of these sensors to acquire imagery even in the presence of cloud cover. Microwave scattering from post-harvest fields is complex, but is driven primarily by soil moisture and surface roughness [10]. In microwave modeling, roughness is represented by the statistical variation of the soil surface indicated by the root mean square (*rms*) and correlation length (*l*). Backscatter increases with increasing roughness. Tilling the soil may increase roughness (as with a first tillage pass on an untilled field) or decrease roughness (for example, secondary or tertiary tillage to prepare the seedbed). [10] linked *rms* roughness to tillage implement type.

Most researchers who have studied the application of radar to tillage mapping have focused on the retrieval of *rms* from backscatter intensity [9], detecting changes in backscatter due to tillage [13], or integrating SAR images in classifiers [11,12]. [9] tilled research plots with different implements and then measured the backscatter (in HH (horizontal send, horizontal receive), VV (vertical send, vertical receive), and VH polarizations, (vertical send, horizontal receive)) with a C-band scatterometer. Using two multivariate models (including soil moisture and roughness) and backscatter measured at two incident angles, *rms* was estimated and plots which were not tilled could be statistically separated from tilled plots. In addition, this modeling approach was able to separate plots tilled with a noble blade, chisel and moldboard plow. Applying change detection, [13] tested whether three dates of RADARSAT-1 C-band imagery could detect if farmers had tilled their fields. Although the change in C-HH backscatter was linked with primary tillage and could be used to separate broad tillage classes, the presence of crop residue also affected scattering. As such, these researchers proposed a framework to classify tillage using both SAR and optical imagery.

More recently [11], combined Sentinel-1 SAR images with optical data (Landsat 5, 7 and 8) to produce annual large-scale maps of the intensity of tillage from 2005 to 2016. Utilizing Google Earth Engine (GEE), these authors generated C-band SAR intensity for VV and VH polarizations and combined these with nine optical spectral indices including: EVI (Enhanced Vegetation Index); GCVI (Green Chlorophyll Vegetation Index), NDVI (Normalized Difference Vegetation Index), cumulated NDVI (SNDVI), NDTI (Normalized Difference Tillage Index), NDI5 & NDI7 (Normalized Difference Index Landsat Band 5 and Landsat Band 7, SWIR (short wave infrared) 1 & 2) and STI (Simple Tillage Index), and texture metrics derived from GCLM (Grey Level Co-Occurrence Matrices) from both the SAR and optical imagery. Overall, the best classifications were achieved with the Landsat derived parameters with accuracies ranging from 75% to 79%, through eleven years of the study. Sentinel-1 backscatter data did not contribute any improvements to the large-scale maps of the intensity of tillage. These findings reflect the challenges in using SAR backscatter alone since not only do changes in roughness impact scattering but so do other soil property changes (i.e., changes in soil moisture and residue).

[12] used a combination of Sentinel-1 and Sentinel-2 data to classify six agriculture classes including conventional plowing (mostly moldboard tillage), conservation tillage, autumn crop, grass, stubble, and stubble with a companion crop. Sentinel-1 SAR VV and VH intensity, and two optical indices from Sentinel-2, were input into several classification techniques including Support Vector Machine (SVM), Multi-Layer Perceptron (MLP), and Random Forest (RF)). RF provided the best overall accuracy at 70% for the six classes.

Techniques such as those described above are considered incoherent methods as they limit analysis to SAR backscatter (intensity or amplitude) and do not directly exploit information about the phase of the wave. Phase can be used to measure the distance from the SAR antenna to (and from) the target. If this distance changes from one SAR acquisition to another as a result of movement of the Earth surface, this will be reflected in a shift in phase. Coherent change detection (CCD) is a technique which uses both the intensity and phase of the scattered wave to detect a target change. When a field is tilled the roughness of the surface is altered (changing the SAR

intensity), but so too is the distance between the SAR antenna and soil surface (changing the phase). Consequently, an image acquired before tillage and an image acquired after tillage would be decorrelated in both phase and intensity.

CCD uses the magnitude of the complex cross correlation of pairs of SAR images to quantify changes in intensity and phase, and this method has demonstrated sensitivity to very subtle changes in the target [14]. The application of CCD requires that image pairs are acquired in the exact same geometry. Any change in distance (e.g., phase) between images is due to a change on the ground and not to a change in the path length travelled by the microwave at differing incidence angles or satellite orbit.

Coherence (γ) can be calculated as [15,16]:

$$\gamma = \frac{|\langle I_1 I_2^* \rangle|}{\sqrt{\langle I_1 I_1^* \rangle \langle I_2 I_2^* \rangle}} \tag{1}$$

where I_1 and I_2 are two complex SAR images (including both phase and intensity) acquired in the exact same geometry from different dates, $|.|$ is the absolute value, $\langle .. \rangle$ is an indication that averaging has occurred, and * is a complex conjugate product. The values of coherence range from 0.0 (complete decorrelation) to 1.0 (complete correlation).

Coherence can be comprised of several components and these are modeled as [16]:

$$\gamma = \gamma_t + \gamma_n + \gamma_{atm} + \gamma_{topo} \tag{2}$$

where γ_t is the temporal coherence component, γ_n is the decorrelation due to receiver noise, γ_{atm} is the decorrelation due to temporal variability in moisture of the troposphere and ions in the ionosphere that cause patterns at spatial wavelengths of 1 km or larger. There can also be contributions due to topography (γ_{topo}) which can be corrected with a digital elevation model (DEM). Decorrelation due to atmosphere can be considered negligible (γ_{atm}) at C-band; (γ_{topo}) can be corrected during pre-processing. Receiver noise causes decorrelation depending on the reflecting signal strengths compared to the noise level (e.g., signal to noise ratio). Each of these are sources of noise that could mask or be confused with the temporal component γ_t, which is of interest in this study. When considering soils, γ_t can then be expressed as:

$$\gamma_t = \gamma_{moisture} \; X \; \gamma_{human \; activity} \tag{3}$$

where $\gamma_{moisture}$ is the contribution to the temporal component from precipitation and from changes in soil moisture, and $\gamma_{human \; activity}$ is the contribution to the temporal coherence from an agriculture management activity that occurs between the two dates of imagery.

CCD is applied to two images, one acquired before and one after land management activity (e.g., $\gamma_{human \; activity}$). The output is a change product with lower coherence values for those fields which were tilled or harvested between image acquisitions. If no further land management activity occurs on the changed fields, the coherence of subsequent image pairs would raise, indicating no further change in intensity or phase. Harvesting and tillage are not the only field activities that can create decorrelation.

[17] used VV coherence to detect and categorize the period of harvesting, and harvesting end dates using Sentinel-1 imagery available every 12 days from May 1st to October 28th. CCD values calculated for each image pair were plotted. Date of harvest could be determined to within 6.5 days using the decline in coherence between images. [15] analyzed 60 Sentinel-1A and B images using VV polarization, acquired every 6 days, over an agriculture area of five crop types including potatoes and sugar beets. Coherence decreased slightly in late September when potato stems and leaves were removed (i.e., haulming period). Coherence increased after that date. The increase in coherence after haulming could be used to estimate when potatoes were harvested as typically, harvest occurs approximately 20 days after haulming. In this case harvest dates were predicted as prior to October 25th for potatoes and by November 30th for beets. [18] evaluated whether Sentinel-1 images with a 12-day repeat could detect when crops were seeded as well as harvested. The authors plotted the time-series of both intensity (VV, VH) and coherence for four crop types (barley, canola, soybean and oats). Seeding (early May) and harvest (approximately September) were determined to have occurred when coherence values for image pairs were low (0.2–0.3) and when the coherence of the next image pair was higher (>0.3) indicating no further change. The periods of higher coherence after the harvest also had lower VH intensity values indicating the removal of the crop and a smoother soil surface.

[16] assessed mowing and plowing events using 386 Sentinel 1A and B products along with Sentinel-2 NDVI and ancillary precipitation data from May to October 2017. These authors related the time-series of Sentinel-1 coherence, using VV and VH polarizations, to Sentinel-2 NDVI. They found that coherence created from both polarizations increased after mowing and plowing events however for plowing, the VV coherence increased more than the VH coherence. This research demonstrates the benefit of a dense time-series of imagery.

Most of the assessments using CCD have focused on determining if coherence can detect seeding [18]; mowing [16,19] and harvesting [15,17,18], while only a few focused-on tillage (plowing) [16]. All of these studies utilized C-band Sentinel-1 data given that this mission delivers a standard coverage yielding a temporal consistency and spatial repeatability desirable for detecting autumn agriculture activity due to seeding, harvesting and tillage.

1.2. Sentinel-1 and the Radarsat Constellation Mission (Rcm) As A virtual constellation

The Committee on Earth Observation Satellites (CEOS) defines virtual constellations as coordinating space-based systems to meet a common set of requirements [20]. Prior to the failure of Sentinel-1B (launched 2016 and failed December 2021), the combination of Sentinel-1A (launched 2014) and Sentinel-1B provided a C-band SAR revisit of 6-days. Over land, the Sentinels typically acquire

Interferometric Wide (IW) mode dual-polarization (VH and VV) data [21]. In 2019 Canada launched the RADARSAT Constellation Mission (RCM), a follow-on to the RADARSAT-1 and RADARSAT-2 C-band missions. With a three-satellite constellation, each RCM satellite has a 12-day revisit, and when all satellites are used together, exact revisit improves to 4 days [22]. RCM is tasked by the Government of Canada and acquires data in a range of modes, polarizations and resolutions. Although the Sentinels and RCM operate with the same centre frequency (5.405 GHz), the nominal orbit height is not consistent between the Sentinels (693 km) and RCM (600 km). The difference in orbit means that an image from Sentinel-1 cannot be combined with an image from RCM, to create a single CCD product. However, CCD products derived from Sentinel to Sentinel, or RCM to RCM pairs could be combined to create a denser time-series. This approach is beneficial considering the loss of Sentinel-1B, degrading a 6-day Sentinel-based CCD product to a 12-day product. A revisit of 12 days introduces complications due to the potential for temporal decorrelation from changing soil moisture. As well, the state of agriculture fields changes frequently due to harvesting, tillage and autumn seeding, and these events may be difficult to resolve with two Sentinel-1A images acquired 12 days apart.

1.3. Objectives

This research explores whether CCD can detect when agricultural fields are tilled. The first objective is to determine if any tillage events, either conservation or conventional tillage, change coherence and if CCD can differentiate change due to tillage from change created by other autumn agriculture activities such as harvesting, autumn seeding and termination of crop with chemical applications. The second objective of the research is to evaluate if the CCD products created from Sentinel-1 image pairs and RCM image pairs can be combined to provide a richer temporal tracking of agriculture activities, thus demonstrating the concept of a virtual constellation for monitoring the uptake of agriculture field activities.

2. Methods

2.1. Study site, field data and earth observation data

The area of interest (AOI) is collectively known as 'Medway' which is located south-west of the town of St. Mary's, Ontario and north of the city of London, Ontario (Canada) (Fig. 1). Two watersheds were assessed including the Upper Medway and the Eastern Medway watersheds. These are both sub-watersheds of the Upper Thames River watershed [23] and within the larger, regional Lake Erie basin. Within the Medway area much of the land is used for agriculture with soybean, corn and wheat representing the majority of the annual cropland. The region has a growing season beginning with seeding around early May and harvest in early October [24] with warm summers and cold, snowy winters. Typically, September has the most precipitation in the region with an average of 61 mm, and the autumn period becomes progressively cloudier ranging from approximately 30 to 40% cloud cover in September to upwards of
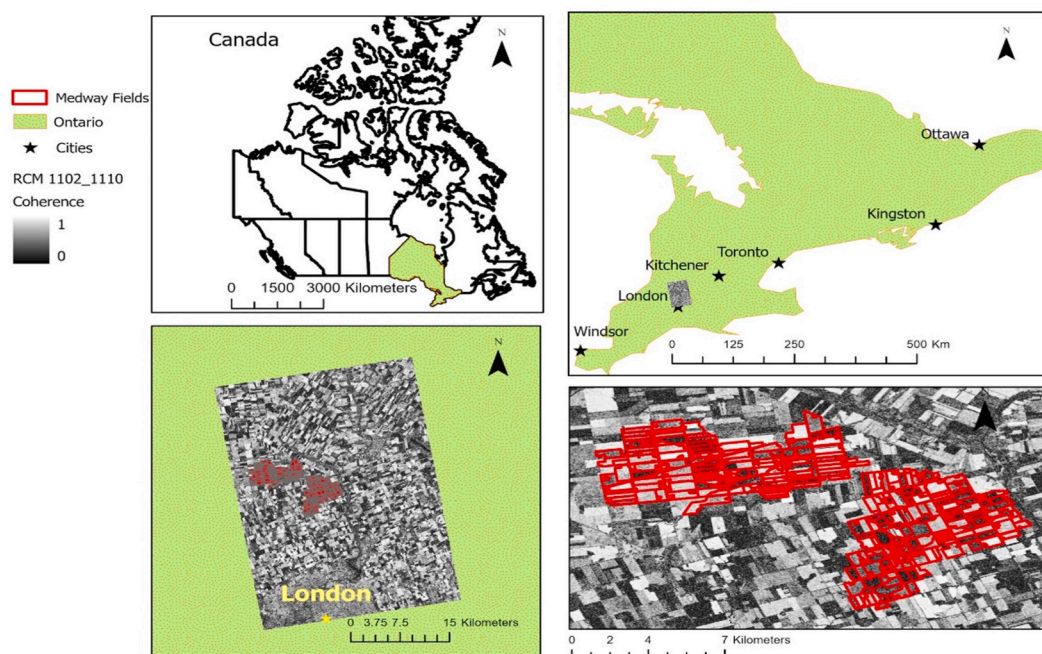
Fig. 1. Area of interest known as Medway, north of London, Ontario (Canada). Green area is the province of Ontario, red outlines are the Upper and Eastern Medway watersheds. (For interpretation of the references to colour in this figure legend, the reader is referred to the Web version of this article.)

70% cloud cover in December [25]. The topography within the region is relatively flat with very minor changes in elevation.

2.1.1. Field data collection

Agronomists completed windshield surveys [26] of both Medway watersheds starting on September 21st, 2021 and continuing approximately weekly until November 26th, 2021. This schedule resulted in a total of 12 in-person visits. Each of the 12 visits were conducted on the same day as the overpass of the Sentinel-1A satellite. On each visit the agronomist noted the current state of the field from a pre-determined classification hierarchy (Fig. 2). The classes are intended to capture a simplified version of field management practices of interest that impact the degree of soil disturbance and cover, and align with windshield survey information being collected by agencies in the region for modelling and programmatic purposes [27,28]. Additional observations were noted including the occurrence of other farming activities such as manure applications, visual assessment of soil moisture status (dry, moist, wet), and estimates of the percent of the soil covered by green vegetation or post-harvest residue. Finally, a photo was taken at the location of the observations and a GPS coordinate was positioned within the field observed.

The classification hierarchy begins with either an observation of Green or Not-green. The secondary level splits the Green class into five main components of Cereals/Grasses, Broadleaves, Mixture of Cereal/Grasses and Broadleaves, Perennials and Other. The Not-green category is divided into three categories: Main Crop Not Harvested, Main Crop Harvested and Tilled. At both levels, the agronomist was asked to provide a visual estimate of the percentage of the soil covered by green and residue. While some observations could be made to categorize green cover at more detailed levels, often the view from the side of the field limited determination of cover to the classes of green and percent cover, main crop not harvested, tilled and percent residue cover, and not tilled and percent residue cover (Fig. 2). The residue categories in the observational hierarchy are consistent with those reported in Ref. [29]. This classification scheme had categories such as ≤29%; 30%–59%; and ≥60% which corresponded to the Farmland Health Check-Up workbook of the OMAFRA Great Lakes Agricultural Stewardship Initiative program [27]. 30% is the typical residue cover amount used to distinguish conservation tillage from conventional tillage. However, residue between 30 and 60% is very difficult to distinguish from the road side [28]. The <10% category in the classification scheme in this research (Fig. 2) is meant to represent conventional tillage and bare soil, and greater than 60% class essentially represents maximum no-tillage residue.

The point observations acquired by the agronomists were subsequently assigned to field polygons that were manually digitized for the Upper Medway and the Eastern Medway watersheds [30]. The average field size was approximately 15 ha with field sizes ranging from just under 1 ha to almost 50 ha in size. In total, observations from 101 fields are used in this analysis, with each field visited 12 times. Autumn farming practices in this region are not consistent and highly variable in terms of timing, therefore in order to capture the autumn agriculture events multiple visits were warranted. This included observations for 40 corn fields, 33 soybean fields, 19 wheat fields and 9 forage fields, which is representative of the cropping mix of the region.

2.1.2. Earth observation data

Sentinel-1A Interferometric Wide (IW) single look complex (SLC) images were downloaded for two orbits, orbit 77 and orbit 150, both of which covered the AOI. These products have a nominal resolution of 30 m and a 250 km swath. The incidence angle range is 41.36°–45.84° (orbit 150) and 30.28°–36.44° (orbit 77). Sentinel-1B did not acquire imagery over this portion of Canada while it was active, however the Sentinel-1A orbit overlap in this region provided an opportunity for a 6-day repeat of Sentinel-1A. Coherence was calculated utilizing the VV polarization. [16] determined that coherence products created using VV were more sensitive to tillage than CCD products from VH. This observation can be explained by the sensitivity of VH to multiple scattering and the lower backscatter (relative to noise floor) of VH for bare soils.

RCM data were programmed over the AOI by tasking all three RCM satellites (RCM1, RCM2 and RCM3) with an 8-day repeat cycle; in one case the repeat was 4-day. The images were acquired in a compact polarization (CP) configuration (in this case, CP10) and delivered as SLC data. CP has been implemented on RCM as a right-handed circular (RHC) transmit with H + V polarizations recorded on return resulting in two polarizations of RH (right hand circular sent, horizontal received) and RV (right hand circular sent, vertical received). Although CP can be implemented on most RCM modes, here CP was tasked in High Resolution mode. This mode has a
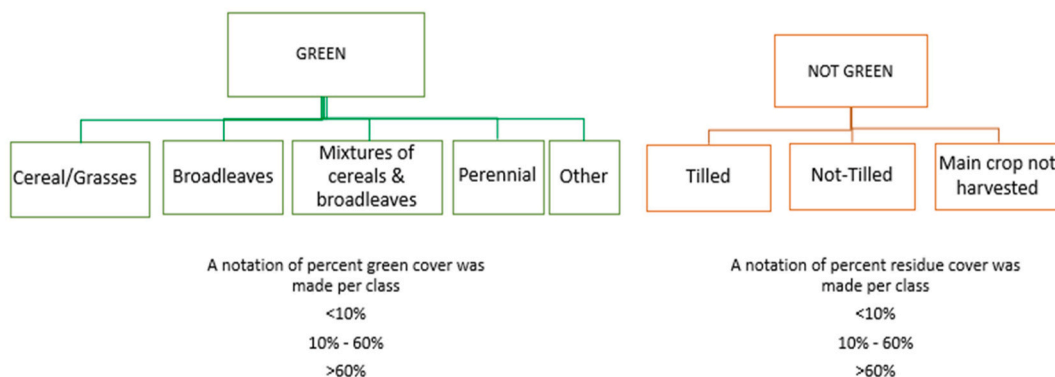
Fig. 2. Field observation hierarchy. Secondary level was the desired observation level although in some cases less detailed observations were made.

nominal spatial resolution of 5 m and an image swath of 25 km. The incidence angle range for 5 m CP mode 10 is 35.27°–37.4°. The Government of Canada is evaluating the calibration performance of the RCM CP modes. The assessment of the High-Resolution CP modes has determined that no additional calibration for non-circularity is necessary for these data [31]. The CP polarization RV was used to calculate coherence images.

Altogether, 14 Sentinel-1A images in two orbits and 12 RCM images were collected, resulting in 23 CCD image products. Table 1 lists the dates of acquisitions and the CCD products created per satellite constellation and per orbit for Sentinel-1A. Each CCD product pair was named as a combination of the month and date each image in the pair was acquired.

2.2. CCD image creation

All SAR images were processed using the European Space Agency's (ESA) SNAP tool version 8.0 [32]. Fig. 3 outlines the general processing steps to generate the CCD images from both sensors. For the Sentinel-1 images an orbit file was applied and images were burst merged and subset to the Area of Interest (AOI) [32,34]. The first step to create the coherence products was to co-register the two SLC images selected to create each CCD image pair. Precise co-registration is important to ensure an accurate calculation of the change in phase between the two images, for each pixel. The co-registration process in SNAP uses a cross-correlation process that collocates a secondary image to a primary reference image ensuring that they both have similar dimensions and geo-positioning. The coarse co-registering process uses orbital data and/or the annotated tie-points. Any offsets between the primary and secondary images are assessed through the maximization of the cross-correlation and then subsequently the secondary pixels are resampled to the primary image using a co-registration polynomial interpolation based upon the offsets. Once the images are co-registered to a single stack the coherence is then calculated following equation (1).

Both the flat Earth phase and the topographic phase (γ_{topo}) were removed through the utilization of the Shuttle Radar Topography Mission (SRTM) 1 arc second DEM [35]. Next, coherence was estimated using a coherence estimation kernel window as noted in equation (1). According to Ref. [16] areas of low coherence contrast can be lost if the kernels are too small. For consistency and to accommodate the potential of inter-comparison of phase coherence estimates from different sensors it is important to use a similar equivalent number of resolution cells in the kernel [16]. For this purpose, approximately 100 samples per kernel were selected while maintaining "square ground dimensions" of each kernel [16]. For the Sentinel-1 processing a window size of 5 in the range and 20 in the azimuth was used, and for RCM a window size of 9 in the range and 13 in the azimuth was selected. Once the CCD image was created in slant range, terrain correction was applied to facilitate the interpretation of coherence using the field observations. A Range-Doppler model was selected for terrain correction [33] with a pixel spacing of 20 m for Sentinel-1 and 10 m for RCM.

Between SAR acquisitions, the state of agriculture fields can change not only as a result of farming activities, but also due to weather events. These extraneous events can also decorrelate coherence between images. Of particular concern are precipitation events (rain and snow) and soil dry down. Daily measures of soil conditions across the site would be needed to identify and model the impact of these events on coherence. Given the absence of these measures, a strategy was developed to flag and remove CCD images which were likely impacted by these changes in soil conditions. To do so, the mean coherence for all pixels in the AOI in the CCD image (the background coherence) was calculated. The assumption was that given the land cover in the AOI, the background coherence should be relatively high. Although farmers were active on their fields, many fields would remain unchanged between SAR acquisitions and other land covers (urban, small water bodies) would remain coherent. However, a weather event (rain or snow) would likely impact most pixels and thus reduce the average image coherence of the entire AOI. Using this strategy, the mean coherence for all pixels in the AOI

Table 1
List of dates of acquisitions for RCM and Sentinel-1 images along with the CCD products created.

RCM Images			
Month (month number)	Day of Month/Satellite		
	RCM 1	RCM 2	RCM 3
September (09)		7, 19	11
October (10)	9	25, 1	17
November (11)	2, 26	18	10
December (12)			4
Sentinel-1A Images			
Month (month number)	Day of Month/Orbit		
	Orbit 77		Orbit 150
September (09)	15,27		8,20
October (10)	9,21		2,14,26
November (11)	2,14,26		7,19
CCD Images			
Sensor/Orbit	Pairs (monthday of image 1_monthday of image2)		
RCM	0907_0911, 0911_0919, 0919_1001, 1001_1009, 1009_1017, 1017_1025, 1025_1102, 1102_1110, 1110_1118, 1118_1126, 1126_1204		
Sentinel-1A 77	0915_0927, 0927_1009, 1009_1021, 1021_1102, 1102_1114, 1114_1126		
Sentinel-1A 150	0908_0920, 0920_1002, 1002_1014, 1014_1026, 1026_1107, 1107_1119		
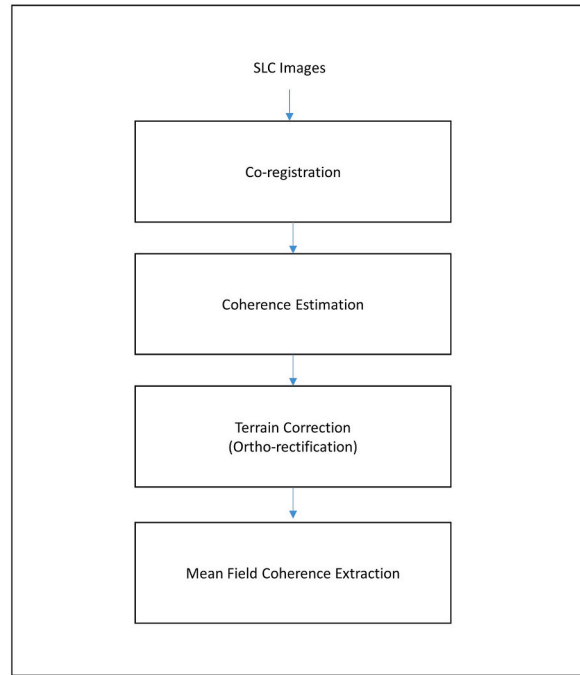
Fig. 3. Coherence image generation steps using ESA's SNAP 8.0.

was calculated for each CCD product. If the mean background coherence value fell at or below 0.20, this CCD product was removed from the analysis. Hourly precipitation data from a nearby weather station, and observations recorded by the agronomists, were used to evaluate the effectiveness of this strategy and to adjust the coherence threshold. An Environment and Climate Change Canada weather station is located near St. Mary's [39] and provides hourly temperature and precipitation. Although imperfect, this approach to quality assessment of the CCD products helped to mitigate confusion between coherence change due to weather events, and change due to agriculture activity.

For the remaining CCD images, mean coherence was extracted for each of the 101 fields, for 16 remaining quality checked CCD pairs. Coherence was plotted by field, and interpreted using the field observations of agriculture activity. This enabled a comparison of the CCD value to the agriculture activity during the particular time periods.

2.3. CP image decomposition

The RCM CP SLC data can also be processed to create additional image products to help interpret scattering responses. Although CCD will detect change, it was important in this research to also develop a method to categorize the type of change (harvest, tillage, autumn seeding). Using fully polarimetric C-band data from the SIR-C mission [36], demonstrated that scattering characteristics varied among unharvested, harvest but untilled, and tilled fields. Polarization plots among these fields varied. Most notably the pedestal height, which is indicative of the degree of polarization (m), was higher for unharvested and untilled fields, decreasing after tillage. Considering these SIR-C results, the m-chi decomposition can be applied to the CP data to categorize scattering. This decomposition allocates total received power into one of three sources of scattering, using intensity (from Stokes parameter S_0), degree of polarization (m) and the ellipticity angle (χ):

$$R^2 (double\ bounce) = m S_0 \left(1 + \sin 2\chi\right) / 2 \tag{4}$$

$$G^2 (volume\ scattering) = S_0 \left(1 - m\right) \tag{5}$$

$$B^2 (single\ bounce) = m S_0 \left(1 - \sin 2\chi\right) / 2 \tag{6}$$

The decomposition was applied to each RCM image using the methodologies described in Ref. [37]. [38] determined that a ratio of Volume to Surface scattering (V/S) was helpful in standardizing scattering responses calculated from decompositions, and this ratio was more sensitive to changes in crop growth. As such, the mean V/S ratio was calculated for each of the 101 fields and each RCM image, using the outputs from the m-chi decomposition.

3. Results & discussion

Table 2 lists the background coherence values for the CCD image pairs used in this research. Four CCD images were set aside from the time-series due to low background coherence, as explained above, most likely due to the impact of environmental factors (rain and snow). Three additional image pairs were set aside from analysis as these didn't coincide with field observations which makes their interpretation more challenging. This resulted in a time-series of sixteen CCD images covering the period from September 21st to December 4th. Fig. 4 provides the location of the 101 observed fields. The location of three fields (yellow) are indicated as these fields were used to plot time-series in Figs. 7–14.

3.1. Overall observations

Of the 101 observed fields, 24 fields were observed to have been tilled at some time during the autumn period. Five of the 24 fields were only partially tilled as farmers left the remainder of the field to be tilled in the spring. The remaining 19 fields were completely tilled. Of the 19 fields that were fully tilled, at some point in the CCD time-series the coherence of 17 of these fields fell below 0.20. Not to be confused with the mean background coherence of the AOI, this localized field level drop in coherence below 0.20 is indicative that a field has been tilled between the first and second images of the CCD image pair. As such, 89.5% of fields (i.e., 17 of 19 fields) observed to have been tilled had a drop in coherence below 0.20 as captured by the CCD image pair.

Of the two fields where the coherence values did not drop below 0.20, one field had an error in the geolocation of the field during autumn field observations by the agronomist. The second field had been tilled, but this change in field condition was not reflected in a low coherence level below 0.20. The cause of this error is unknown, but it was speculated that it could be related to geolocation issues, artifacts in the SAR imagery, or related to some unobserved process that the farmer undertook during this time period.

Fig. 5 box plot graphs the coherence values for all 16 CCD products, for the observed fields (1616 observations). The X represents the mean value of each plot, while the bars represent the range of values per box plot. The dots are representative of outliers. Of those 1616 observations 1344 represented no change and 85 represented change. The remaining 187 observations were related to when the field had green vegetation cover as a result of continued growth of the main season crop, an overwinter cover crop or weeds. These green cover fields were discarded from further analysis. The field level coherence values are categorized according to whether the agronomists noted change or no change in field conditions due to harvest, tillage or autumn seeding for each field and CCD product.

There is a clear separation between the two classes, as observed in Fig. 5. The mean and standard deviation of the coherence for fields that had not changed was calculated, and was found to be 0.42 ± 0.15. The mean and standard deviation for fields that experienced change was also calculated, and was found to be much lower at 0.18 ± 0.03. The difference between these results demonstrate that autumn farming activities can be detected using CCD. Overall, when comparing CCD values, field level coherence fell below 0.20 for the majority of these changed fields, confirming that the correlation in amplitude and phase from image 1 to image 2 decreases. This decorrelation is attributable to changes in biomass after harvest or roughness due to tillage (affecting scattering intensity) and changes in the height of the target following these events (affecting phase). For almost all the fields and observation dates where no change was recorded, the field average CCD values were all above 0.20.

Fig. 6 is a box plot that breaks down the distribution of the CCD values for different types of farming activity. This figure expands the change category from Fig. 5 (blue box plot). Classes are separated by crop type (corn, soybean and wheat) and tillage status (tilled or not tilled). There were no observations of wheat or forage harvesting as the wheat harvest in this region occurred earlier than the first date of observation, September 21st, and the cutting of forage did not occur during the observation period. Only one of the observed fields of forage was tilled. With only one data point this field was removed at this point from any further analysis.

As described in Ref. [29] the timing of harvesting and tillage activities in this region of the Lake Erie basin varies depending upon

Table 2
List of the CCD images created and analyzed in this research. The mean background coherence values for the AOI are provided for each CCD pair.

Satellite/orbit	daymonth image1_daymonth image2	Mean background coherence
S-1A Orbit 150	0920_1002	0.2406
	1002_1014	0.3299
	1014_1026	0.4070
	1026_1107	0.3969
	1107_1119	0.4190
S-1A Orbit 77	0927_1009	0.2981
	1009_1021	0.3375
	1021_1102	0.3428
RCM	0911_0919	0.2339
	0919_1001	0.2757
	1001_1009	0.3121
	1009_1017	0.3299
	1017_1025	0.3050
	1102_1110	0.4508
	1118_1126	0.3420
	1126_1204	0.3248
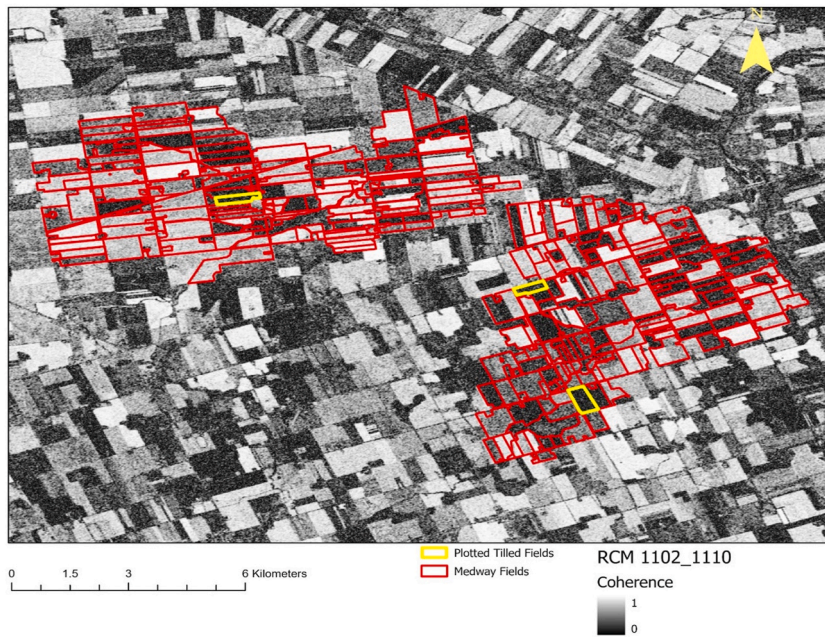
Fig. 4. Location of the 101 observed fields (red); yellow outlined fields are the three examples presented in the following analyses; background is the RCM Nov2_Nov10_Oct17 CCD image. Fields with high coherence are brighter and those with low coherence (suggesting change in field conditions) are darker. (For interpretation of the references to colour in this figure legend, the reader is referred to the Web version of this article.)
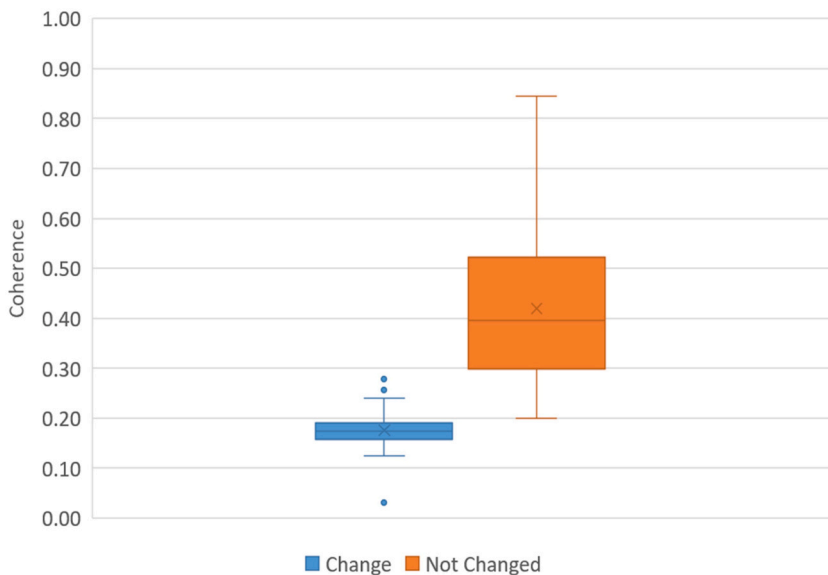
Fig. 5. Comparison between the CCD values for fields and dates where change and no change were documented in field observations. The mean and standard deviation for change was 0.18 ± 0.03 Std and for not changed 0.42 ± 0.15 Std.

crop type. When corn or wheat are harvested, field level coherence falls below 0.20 (Fig. 6). Some, but not all, soybean fields drop below 0.20 due to harvest. A Kruskal Wallis H Test was performed to test the statistical significance of differences among the five classes (Corn Tilled, Corn Harvested, Soybean Tilled, Soybean Harvested and Wheat Tilled). This statistical test compares the median among these groups and determines if any of these class medians are statistically different. This test is used instead of a single-factor ANOVA when data are not normally distributed and have non-similar variances. The results indicated that for at least two of these five classes, CCD median values were statistically different (p-value <0.05). To further investigate which specific classes were statistically separable, we applied a Fisher's least significance difference (LSD) pairwise comparison at a 5% probability level [40,41] (Table 3).

For the corn class, there was a significant difference in CCD response between fields tilled and those harvested. This result was also
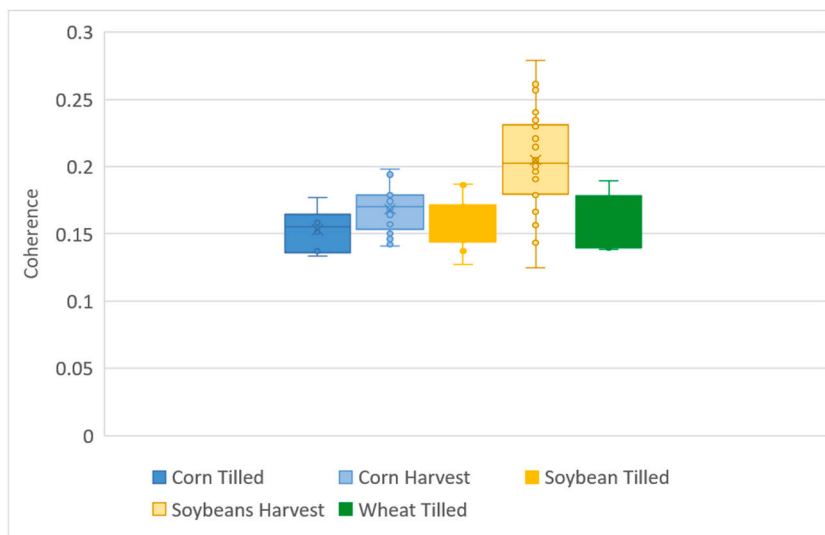
Fig. 6. Comparison among the field level CCD values for the changed fields where farming activity has occurred. Change is partitioned by crop type and agriculture activity: tillage or harvesting.

observed for soybeans. For wheat, the harvest period was not captured during field work. CCD values were also significantly different between the Corn Harvest and Soybean Harvest classes. In summary, coherence values could separate fields that were tilled from fields that were harvested, for corn and soybeans, and CCD could separate harvest as a function of crop type (corn or soybeans). However, CCD alone was not be able to distinguish between the following classes: Soybean Tilled and Corn Tilled; Soybean Tilled and Wheat Tilled; Wheat Tilled and Corn Tilled). It may be possible to use ancillary data, such as crop inventory maps, to identify the crop type (and thus residue type) in order to separate these classes.

3.2. CCD time-series trends of specific corn, soybean and wheat fields

In addition to these summary statistics the trend in field level coherence prior to, at the time of and after harvest and tillage, is informative. The time-series of coherence for three fields (one for each crop type of corn, soybean and wheat) is graphed in Figs. 7–13. Fig. 7 includes separate graphs for the coherence derived from Sentinel-1 image pairs (7a), and RCM image pairs (7b), for a selected corn field. A time-series that combines coherence products from both Sentinel and RCM satellites is graphed in Fig. 8, for this same field. Comparing Figs. 7 and 8 demonstrates that combining coherence products from both of these constellations provides more temporally rich information as a denser time-series reduces the risk that farming activities will be missed.

In Fig. 8, a decline in coherence is observed from the approximate date of maturity to harvest. Field crews noted that this field was harvested on October 26th. This decline from approximately 0.76 to 0.53 (from maturity to harvest) represents a relative decrease in coherence of 30%. In Ontario, corn reaches physiological maturity from late September to early October with moisture levels at this stage of development typically around 30% [42]. Dry down from maturity will see corn lose 0.4–0.6% moisture per day and it can take three to four weeks for corn to dry to an optimal moisture for harvest (around 18%) [42]. From the perspective of microwave scattering, this slow but steady dry down will change the intensity of backscatter (due to declines in canopy water), but will also move the location of the scattering phase center. According to Ref. [43] for vegetation, the scattering phase center will lie at or above the ground (depending on microwave frequency) and this location within the canopy will depend upon the vegetation attributes.

At C-band, scattering is expected to be predominately within the canopies of large biomass crops like corn. Scattering within the canopy, even just prior to harvest when vegetation moisture is approximately 18%, is confirmed in Fig. 9. The V/S ratio remains high (above 2, indicated as ● "right before harvest" in Fig. 9) indicating that contributions from volume scattering within the corn canopy still dominate over surface scattering contributions from the soil even when the canopy water has declined. This observation is unsurprising given the relative size of a C-band wave (~5 cm) and the typical height of corn at maturity (~3 m). The penetration depth

Table 3
Results of Fisher's LSD test. Class comparisons labeled as significant (bolded) indicate that CCD values were statistically separable at a 5% probability level. Bolded and underlined results indicate that CCD was able to separate harvest events and tillage events, within a specific crop category.

	Corn Tilled	Corn Harvest	Soybean Tilled	Soybean Harvest
Corn Harvest	**<u>Significant</u>**			
Soybean Tilled	Not Significant	Not Significant		
Soybean Harvest	**Significant**	**Significant**	**<u>Significant</u>**	
Wheat Tilled	Not Significant	Not Significant	Not Significant	**Significant**
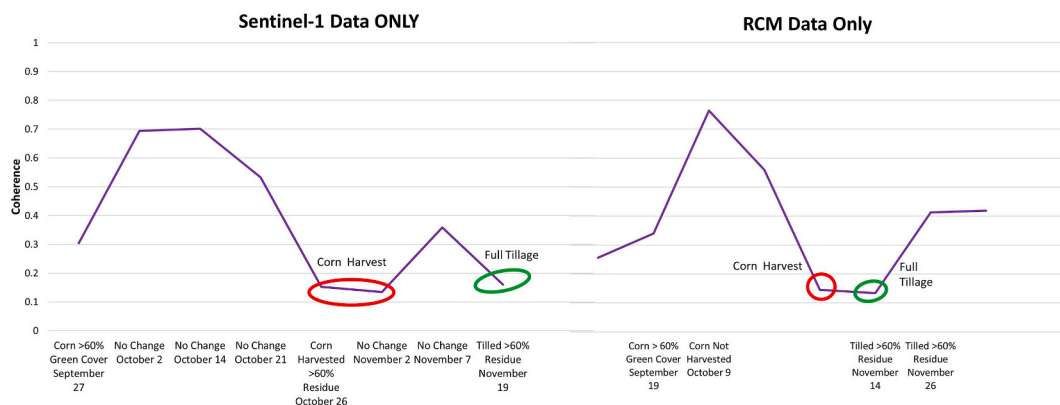
Fig. 7. a) Coherence time-series from only Sentinel-1A data, b) Coherence time-series from only RCM data. These plots are for one corn field in the Medway watershed.
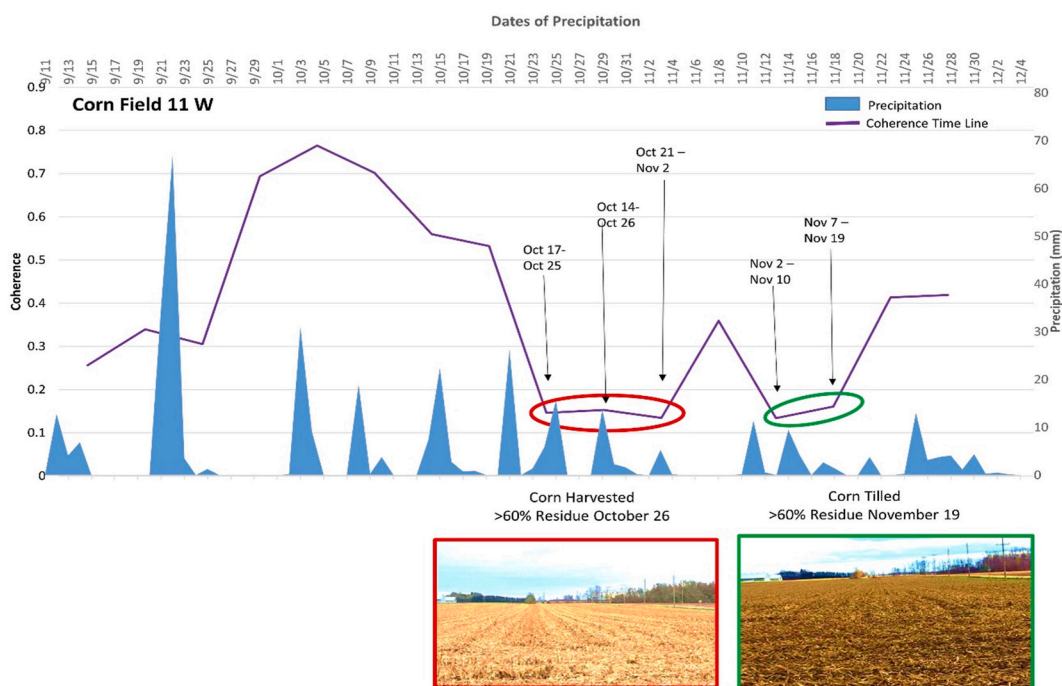
Fig. 8. Sentinel-1A and RCM CCD time-series for a corn field (purple line). Precipitation is captured on the secondary axis (in blue) and red circles/outlines are dates of harvest and green circles/outlines are dates of tillage. (For interpretation of the references to colour in this figure legend, the reader is referred to the Web version of this article.)

and the location of the scattering phase center will change as canopy moisture changes, and a decrease in canopy moisture will result in deeper penetration. We hypothesize that the relative decline in coherence of this field by 30% after maturity but prior to harvest, is likely caused by a change in the center of scattering as the canopy loses water (affecting phase) as well as a change in backscatter intensity.

Both the Sentinel-1 and RCM time-series (Figs. 7 and 8) capture corn harvest as a significant relative decrease in coherence (from approximately 0.53 to 0.15; 72% relative decline). This reduction in field level coherence due to harvest confirms Sentinel-1 observations reported by Ref. [18]. When coherence and V/S ratio scattering are plotted for this corn field (Fig. 9), the decline in coherence is evident for harvest (from above 2 to just over 1.5), but volume scattering still dominates from the residue left after this crop is harvested.

When corn is harvested for grain, only the corn kernels are harvested and the remainer of the vegetation matter is left on the field. Although this type of residue can create volume scattering, the height has changed from standing ~3 m high "dry" corn plants (right before harvest) to residue (stalks cut to a few cm in height and leaves covering soil) and the phase will change.

Fig. 9. A scatter plot of coherence compared to the Volume/Surface ratio for a corn field. Points which fall in the grey zone have coherence values less than 0.2, the threshold for field level change; points in green are conditions where surface scattering equals or exceeds the contribution of volume scattering. (For interpretation of the references to colour in this figure legend, the reader is referred to the Web version of this article.)

Subsequently, this field remained untilled for approximately two weeks (early to mid November) and with the field conditions unchanged, the Sentinel-1 coherence increases above 0.20 (Fig. 8). The farmer tilled this field early in November. Coherence fell below 0.20 and in addition, contributions from surface scattering were equal to those from volume scattering (e.g., V/S ratio close to 1) (Fig. 9). Coherence increased above 0.20 after tillage which indicating that this field will be left in this state, leading into winter. During the period of inactivity, coherence values after the harvest and tillage increased although values were lower (0.36) after harvest relative to coherence values after the tillage (0.41). These results are similar to those reported by Ref. [16].

As indicated in Fig. 6, harvesting of soybeans did not reduce coherence below 0.20 for all fields. Even for the field selected for
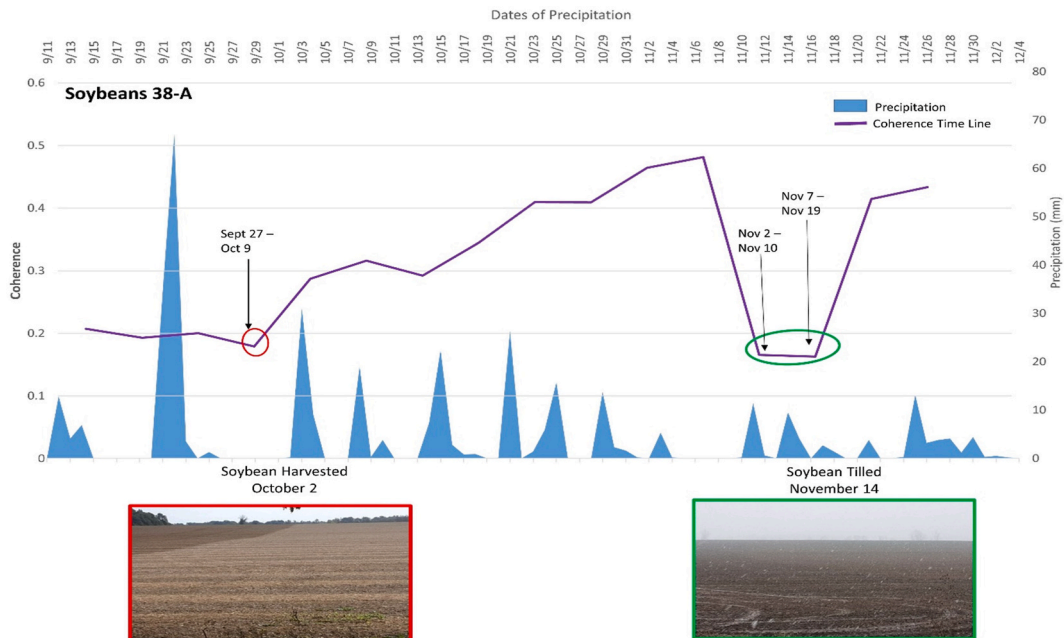
Fig. 10. Sentinel-1A and RCM CCD time-series for a soybean field (purple line). Precipitation is captured on the secondary axis in blue and red circles/outlines are dates of harvest and green circles/outlines are dates of tillage. (For interpretation of the references to colour in this figure legend, the reader is referred to the Web version of this article.)

Fig. 10, coherence dips only slightly below this threshold when this field is harvested. During the active growing season, soybeans never accumulate fresh plant biomass per unit area at the scale of corn or wheat [38]. When soybeans undergo senescence, leaves first turned brown and then fall from the stem. The stems of dry soybean canopies are thin and hollow, having little moisture or weight. At the end of senescence when the crop is ready to harvest soybean canopies have lost almost all leaves and what remains is the stem with dried pods and seeds. For the most part, microwaves would penetrate this dried soybean canopy. It is unsurprising that harvesting of soybeans would have a much smaller impact on coherence. There would be little scattering differences and height differences in terms of the pre-harvested senescence soybean plant's structure and form, and remaining residue after harvest.

After harvest, coherence increases steadily as the field is left untouched prior to the date of tillage. Soybeans leave little post-harvest residue given their low biomass at harvest and the field, as with corn, stays in a steady state until tillage is applied. This field remained untilled during this approximately one-month period. The tillage event was captured by the CCD images of 1102_1110 and 1107_1119 (Fig. 10). Here, the relative change in coherence is similar to that observed for corn (Fig. 8). Field level coherence for this soybean field fell from 0.48 to 0.17, a relative decline of 65%, when tillage was applied. Similar to the corn time-series, the coherence values increase after both the harvesting event (0.29) and the tillage event (0.41). Detecting the harvesting of soybeans using CCD is not obvious given the small decline in coherence. Fig. 11 graphs the change in coherence over time, when the coherence values of the soybean field from one CCD product are compared to the values of the prior CCD pair. Change in CCD values over time remains close to zero with only small changes above and below this threshold.

In contrast, the tilled field is easily detected around November 10th when the coherence in the difference time-series drops significantly. This decline in coherence is calculated using CCD products created by both Sentinel-1 1026_1107 and RCM 1102_1110.

The wheat time-series (Fig. 12), was different from the other two crop types which reflects the fact that management practices applied to wheat are unique. Specifically, wheat in this region is harvested before early September and in approximately 15 out of the 21 wheat fields that were observed, green vegetation began to emerge after harvest. This green cover was a result of the planting of an autumn over-winter crop, or the emergence of weeds or volunteer wheat (due to seeds falling on the field during harvesting activities). In approximately 8 of the fields, chemical termination was applied which caused this green vegetation to die off. In Fig. 12, coherence declined following chemical termination, documented in the field observations of September 27th, October 2nd and October 9th. Coherence fell to 0.18 on the last date of decline due to chemical termination. Values subsequently increased to 0.42 indicating that between October 9th and date when the field was tilled (November 14th), the state of the field remained unchanged. For coherence, higher coherence values indicate that the target is not changing. If the first CCD pair values are low, and then coherence values increase on the next CCD pair, that generally indicates that change is not occurring on the ground. The CCD products created from November 2nd and November 10th (RCM) and November 7th and November 19th (Sentinel-1 orbit 150) captured a decrease in coherence below 0.20 which is because the field has been tilled. The relative decline in coherence due to the tilling of this wheat field (drop from 0.52 to 0.13 or 75% relative decline) was similar to that observed for corn (62%) and soybean (65%). As observed with corn and soybeans after tilling, this field also remained unchanged moving into winter, with coherence increasing to 0.38.

The field level coherence values for this wheat field increased after both the field was tilled and chemical termination was applied. These relative increases in coherence were similar and as such using only coherence change, it would be difficult to determine which agriculture practice preceded the increase in coherence.
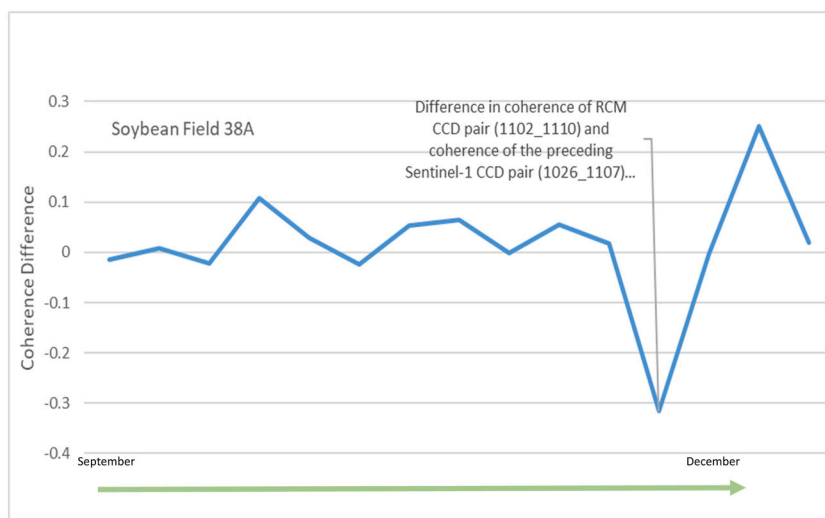
Fig. 11. Sentinel-1A and RCM CCD difference time-series for soybean field (blue line). This graph is created by calculating the difference between the coherence of one CCD pair and the coherence of its preceding CCD pair. (For interpretation of the references to colour in this figure legend, the reader is referred to the Web version of this article.)
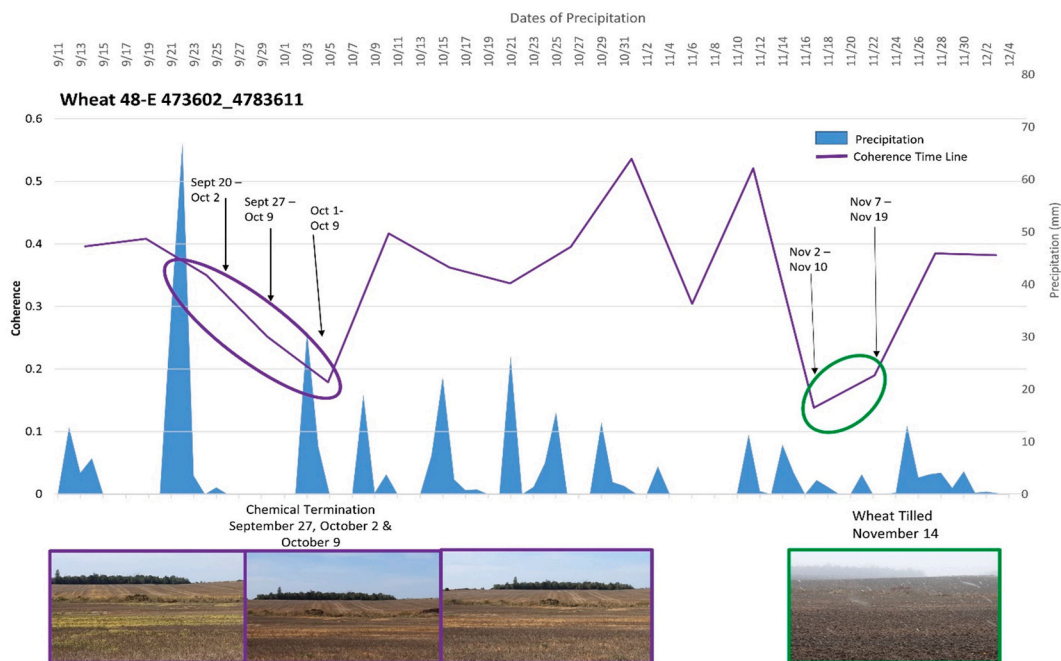
Fig. 12. Sentinel-1A and RCM CCD time-series for wheat field (purple line). Precipitation is captured on the secondary axis in blue and purple circles/outlines are dates of chemical and green circles/outlines are dates of tillage. (For interpretation of the references to colour in this figure legend, the reader is referred to the Web version of this article.)

Additional information would help differentiate these events. [16] used NDVI from Sentinel-2 imagery for this purpose, but for this study optical images were not available after November 10th due to the excessive cloud cover present in this region during autumn months.

Fig. 13 plots the coherence time-series (primary y-axis, line) for this wheat with the V/S scattering ratio values (secondary y-axis, points) derived from the m-chi decomposition. Just prior to chemical termination the V/S ratio value is approximately 1.5 which shows that volume scattering is slightly more dominant than surface scattering. After chemical termination the V/S values decreased to one. This indicates that volume scattering is still present, but becoming more equal to surface scattering. This observation is consistent with a chemical termination, which kills the living plant, but leaves the dead plant matter. This dead plant matter, as with crop residue, still retains enough vegetation water to create some scattering. However, after the field is tilled the V/S values declined to below one as plant matter is buried during the tillage process, and surface scattering from the soil begins to dominate.

Interpreting changes in coherence with changes in volume to surface scattering illustrates that secondary SAR parameters can be beneficial to further define the agriculture practices creating change. These secondary SAR parameters could be used with coherence in a classifier in future research to help map classes of autumn agriculture activity.

Figs. 8, 10 and 12 illustrate a drop in coherence due to harvest (Figs. 8 and 10) and due to tillage (all three). Although these observations are informative, it is also important to determine the date of these farming activities with greater temporal precision. To assist in narrowing the timing of these activities, we created a temporal graphical overlay of CCD pairs for these three fields where coherence was less than 0.20 (Fig. 14). For the corn field, when all three CCD pairs are interpreted together, the timing of harvest is narrowed to between October 21st and October 25nd. This is consistent with observations from the field. On October 26th the field crew noted that this corn field was harvested (Fig. 8, red photo outline). The crew visited this field five days earlier and observed that on October 21st this corn field had not been harvested. With three CCD pairs, harvesting of this corn field is determined to have occurred within this 5 day window. Farmers have a narrow window of time to complete harvest and tillage prior to autumn freeze up. It is possible that although the field crew noted that the field was not harvested on October 21st, the farmer harvested this field on this day but after the field observation, or harvested sometime in the following four days. The approach taken in Fig. 14 improves upon results by Ref. [17] who were able to determine harvest dates to within 6.5 days, albeit using the 12-day repeat of one of the Sentinel-1 satellites. This analysis underscores the importance of increasing the temporal repeat of SAR satellites for CCD applications. More frequent acquisitions lead to great specificity on timing of events which change coherence. In the research presented here, based upon the virtual Sentinel-1 & RCM constellation timeline only one CCD pair captured the soybean harvest. If there had been additional CCD pairs to include perhaps a more refined harvest date could be determined.

This also highlights the importance of other additional virtual SAR satellites that could add more information to the time series.
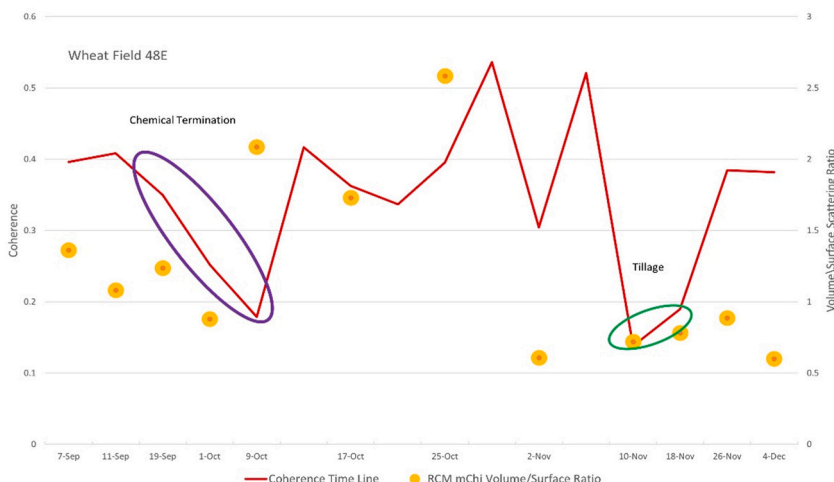
Fig. 13. Coherence time-series (red line) with m-chi V/S ratio (orange dots) for a wheat field. Purple circles/outlines are dates of chemical and green circles/outlines are dates of tillage. (For interpretation of the references to colour in this figure legend, the reader is referred to the Web version of this article.)
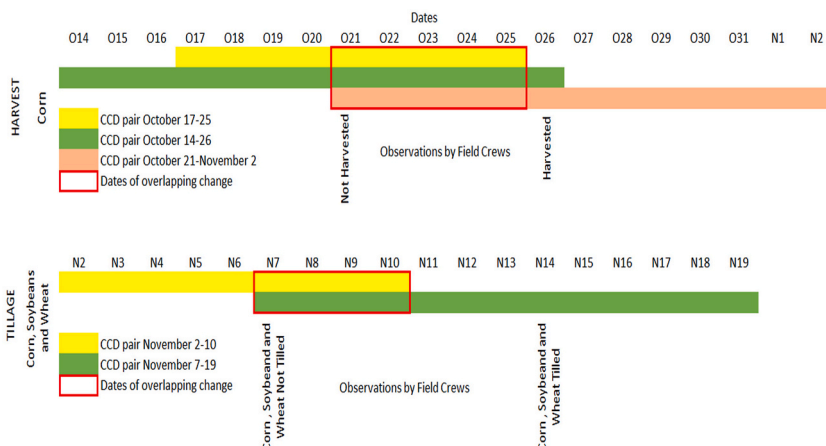
Fig. 14. Overlay of CCD pairs with values less than 0.20. Timing of corn harvest is determined using three CCD pairs (top). Timing of tillage for corn, soybeans and wheat is determined using two CCD pairs (bottom). Dates are indicated as O (October) or N (November). The time period of overlap is outlined in red. Timing of field observations is indicated. (For interpretation of the references to colour in this figure legend, the reader is referred to the Web version of this article.)

4. Conclusions

When agricultural fields are tilled, soil disturbance can reduce soil health and lead to off-site impacts on water systems. As such, farmers are encouraged to adopt Beneficial Management Practices (BMPs) such as no-till, reduced tillage and conservation tillage. Mapping and measuring the uptake of BMPs is a challenge given the large regions of the watersheds of interest, including the Canadian Lake Erie basin. SAR satellites have the capability to collect data repeatedly, over large swaths and during all-weather events, which is an important advantage for this application given that autumn agricultural activities occur with high temporal frequency and at a time when the probability of cloud cover is high.

This research found that autumn agriculture activities, or 'change' events, led to low coherence values (0.18 ± 0.03). For fields that remained 'unchanged' CCD values were higher (0.42 ± 0.15). Statistical tests confirmed that the coherence values associated with unchanged and changed fields was significantly different. More specifically, 89.5% of fields observed as having been tilled had CCD values below 0.20. For the two fields that did not conform to this, one observation had associated field error and the other was suspected to either also have field observation error or SAR image artifacts. CCD was also shown to separate harvested corn fields from harvested soybean fields. The relative decline in coherence before wheat and soybeans tillage events (75% for wheat and 65% for soybeans) was greater than the decline before harvest events, but for corn the relative decline was 72% prior to harvest and 62% prior to tillage. This could be related to the relative short time period between these events for corn (~1–3 weeks) as opposed to those for

soybeans (~4–6 weeks) and wheat (unknown). The V/S scattering ratio declined after all tillage events whereas these values increased after both harvesting and chemical termination. This observation underscores the value of addition ancillary SAR information in differentiating autumn agriculture activities detected using CCD. Additionally, it suggests that the use of these types of variables in a classifier together may help to map classes of autumn agriculture activities which will be considered in future research. Importantly, this study illustrated the value of combining data from different satellite platforms, in a virtual constellation. To more precisely define a window of time when harvest and tillage occurred, Sentinel-1 and RCM CCD products with values below 0.20 were graphically overlaid, and narrowed of the timing of corn harvest to a 5-day window and of the timing of tillage (corn, soybeans and wheat) to a 4-day window. It is believed that with the addition of other satellites' CCD products in a virtual constellation these windows could be narrowed even further and will be the focus of future research.

This research demonstrated that CCD can capture changes in SAR responses (intensity and phase) due to autumn agricultural activities. Using data from multiple sensors increases the density of time-series which is needed to more precisely determine the dates when farming activities occur. Given the positive outcome of the study, it will be helpful to validate these methods for other sites and years. In addition, this study exploited C-band sensors given ready access to data from these satellites. It will be interesting to test the added value of including CCD products from other SAR frequencies, including X- and L-band.

Author contribution statement

Laura Dingle Robertson, Heather McNairn, Marco van der Kooij, Xianfeng Jiao, and Pamela Joosse: Conceived and designed experiments, and analyzed and interpreted the data.

Laura Dingle Robertson, Heather McNairn, and Marco van der Kooij: Performed the experiments.

Laura Dingle Robertson, Heather McNairn, Marco van der Kooij, Xianfeng Jiao, Samuel Ihuoma, and Pamela Joosse: Contributed reagents, materials, analysis tools or data.

Laura Dingle Robertson and Heather McNairn: Wrote the paper.

Data availability statement

The RCM SAR data used in this research is accessible through Natural Resource Canada's Earth Observation Data Management System. The field data may be available upon request.

Additional information

No additional information is available for this paper.

Declaration of competing interest

The authors declare that they have no known competing financial interests or personal relationships that could have appeared to influence the work reported in this paper.

References

[1] W. He, J.Y. Yang, C.F. Drury, W.N. Smith, B.B. Grant, Ping He, B. Qian, Wei Zhou, G. Hoogenboom, Estimating the impacts of climate change on crop yields and N2O emissions for conventional and no-tillage in Southwestern Ontario, Canada, Agric. Syst. 159 (2018) 187–198, https://doi.org/10.1016/j.agsy.2017.01.025.

[2] W. Hassan, Y. Li, T. Saba, F. Jabbi, B. Wang, A. Cai, J. Wu, Improved and sustainable agroecosystem, food security and environmental resilience through zero tillage with emphasis on soils of temperate and subtropical climate regions: a review, Int. Soil Water Conserv. Res 10 (3) (2022), https://doi.org/10.1016/j.iswcr.2022.01.005.

[3] Z. Kabir, Tillage or no-tillage: impact on mycorrhizae, Can. J. Plant Sci. 85 (1) (2005) 23–29, 10.4141/P03-160.

[4] H.M. Beach, K.W. Laing, M. Van De Walle, R.C. Martin, The current state and future directions of organic No-till farming with cover crops in Canada, with case study Support, Sustainability 10 (2) (2018) 373, https://doi.org/10.3390/su10020373.

[5] S. Rasouli, J.K. Whalen, C.A. Madramootoo, Review: reducing residual soil nitrogen losses from agroecosystems for surface water protection in Quebec and Ontario, Canada: best management practices, policies and perspectives, Can. J. Soil Sci. 94 (2) (2014) 109–127, https://doi.org/10.4141/cjss2013-015.

[6] ECCC, USEPA, 2019-2023, Environment and Climate Change Canada and the U.S. Environmental Protection Agency), vol. 120, Lake Erie Lake wide Action and Management Plan, 2021. ISBN 978-0-6660-37577-9.

[7] ECCC, OMECC, Environment and Climate Change Canada and Ontario Ministry of the Environment and Climate Change), Canada-Ontario Lake Erie Action Plan, Partnering on Achieving Phosphorus Loading Reductions to Lake Erie from Canadian Sources, vol. 84, Queen's Printer for Ontario, 2018.

[8] Ontario Ministry of Agriculture, Food and Rural Affairs, (OMAFRA), Governments Improving Water Quality and Farming Around Lake Erie, news.ontario.ca/en/release/1000989/governments-improving-water-quality-and-farming-around-lake-erie, 2021 accessed June 2022).

[9] H. McNairn, J.B. Boisvert, D. Major, Q.H.J. Gwyn, R.J. Brown, A. Smith, Identification of agricultural tillage practices from C-band radar backscatter, Can. J. Rem. Sens. 22 (1996) 154–162.

[10] T.J. Jackson, H. McNairn, M.A. Weltz, B. Brisco, R.J. Brown, First order surface roughness correction of active microwave observations for estimating soil moisture, IEEE Trans. Geosci. Rem. Sens. 35 (1997) 1065–1069, https://doi.org/10.1109/36.602548.

[11] G. Azzari, P. Grassini, J.I. Rattalino Edreira, S. Conley, S. Mourtzinis, D.B. Lobells, Satellite mapping of tillage practices in the North Central US region from 2005 to 2016, Remote Sens. Environ. 221 (2019) 417–429, https://doi.org/10.1016/j.rse.2018.11.010.

[12] M. Luotamo, M. Yli-Heikkilä, A. Klami, Density estimates as representations of agricultural fields for remote sensing-based monitoring of tillage and vegetation cover, Appl. Sci. 12 (2022) 679, https://doi.org/10.3390/app12020679.

[13] H. McNairn, D. Wood, Q.H.J. Gwyn, R.J. Brown, R.J. Mapping tillage and crop residue management practices with RADARSAT, Can. J. Rem. Sens. 24 (1998) 28–35.

[14] M. Preiss, N.J.S. Stacy, Coherent Change Detection: Theoretical Description and Experimental Results, Defence Science and Technology Organisation, Commonwealth of Australia, 2016, pp. 1–116. https://apps.dtic.mil/sti/pdfs/ADA458753.pdf.

[15] S. Khabbazan, P. Vermunt, S. Steele-Dunne, L. Ratering Arntz, C. Marinetti, D. van der Valk, L. Iannini, R. Molijn, K. Westerdijk, C. van der Sande, Crop monitoring using sentinel-1 data: a case study from The Netherlands, Rem. Sens. 11 (16) (2019) 1887, https://doi.org/10.3390/rs11161887.

[16] K. Voormansik, K. Zalite, I. Sünter, T. Tamm, K. Koppel, T. Verro, A. Brauns, D. Jakovels, J. Praks, Separability of mowing and ploughing events on short temporal baseline sentinel-1 coherence time series, Rem. Sens. 12 (2020) 3784, https://doi.org/10.3390/rs12223784.

[17] O. Kavats, D. Khramov, K. Sergieieva, V. Vasyliev, Monitoring harvesting by time series of sentinel-1 SAR data, Rem. Sens. 11 (21) (2019) 2496, https://doi.org/10.3390/rs11212496.

[18] J. Shang, J. Liu, V. Poncos, X. Geng, B. Qian, Q. Chen, T. Dong, D. MacDonald, T. Martin, J. Kovacs, D. Walters, Detection of crop seeding and harvest through analysis of time-series Sentinel-1 interferometric SAR data, Rem. Sens. 12 (10) (2020) 1551, https://doi.org/10.3390/rs12101551.

[19] M. De Vroey, J. Radoux, P. Defourny, Grassland mowing detection using sentinel-1Time series: potential and limitations, Rem. Sens. 13 (3) (2021) 348, https://doi.org/10.3390/rs13030348.

[20] Committee on Earth observation satellites (CEOS), virtual constellations. https://ceos.org/ourwork/virtual-constellations/, 2022 access July 2022.

[21] European Space Agency (ESA), Sentinel-1, https://sentinel.esa.int/m, 2022. accessed April 2023.

[22] Canadian Space Agency, RADARSAT Constellation Mission, 2023. https://www.asc-csa.gc.ca/eng/satellites/radarsat/. accessed April 2023.

[23] Upper Thames River Conservation Authority (UTRCA), Medway Creek, (thamesriver.on.Ca/education-Community/watershed-Friends-Of-Projects/medway/), 2022 (accessed July 2022).

[24] Ontario Ministry of Agriculture, Food and rural affairs (OMAFRA), climate zones and planting dates for vegetables in Ontario. www.omafra.gov.on.ca/english/crops/facts/climzoneveg.htm, 2016 accessed July 2022.

[25] Weather Spark, Climate and average weather year round in London (weatherspark.com/y/18239/Average-Weather-in-London-Canada-Year-Round#:~:text=In%20London%2C%20the%20summers%20are,or%20above%2087%C2%B0F). https://sis.agr.gc.ca/cansis/publications/surveys/on/on56/on56-v1_report.pdf, 2022 accessed July 2022.

[26] F. Waldner, D. De Abellleyra, S.R. Verón, M. Zhang, B. Wu, P.D. Bartalev, S. Lavreniuk, et al., Towards a set of agrosystem-specific cropland mapping methods to address the global cropland diversity, Int. J. Rem. Sens. 37 (14) (2016) 3196–3231, https://doi.org/10.1080/01431161.2016.1194545.

[27] Ontario Ministry of Agriculture, Food and rural affairs, (OMAFRA), great lakes agricultural stewardship initiative: the Farmland health check-up workbook. Guelph, Ontario, Canada: Ontario soil and crop improvement association". http://www.ontariosoilcrop.org/wp-content/uploads/2015/07/Farmland-Health-Check-Up-Workbook-Fillable-PDF.pdf, 2015 accessed July 2022.

[28] N. Pilger, A. Berg, P. Joosse, Semi-automated roadside image data collection for characterization of agricultural land management practices, Rem. Sens. 12 (2020) 2342, https://doi.org/10.3390/rs12142342.

[29] A. Laamrani, P. Joosse, H. McNairn, A. Berg, J. Hagerman, K. Powell, M. Berry, Assessing soil cover levels during the non-growing season using multitemporal satellite imagery and spectral unmixing techniques, Rem. Sens. 12 (9) (2020) 1–18, https://doi.org/10.3390/rs12091397.

[30] Upper Thames River Conservation Authority (UTRCA), Upper_Medway_Land_Use_Layers_GDB, Produced Using Information under License with the Upper Thames River Conservation Authority © Upper Thames River Conservation Authority, 2021.

[31] R. Touzi, M. Lapointe, S. Nedelcu, M.A. Fobert, S. Cote, Assessment and Calibration of RCM Compact, Proceedings of the 42 Canadian Symposium on Remote Sensing, Virtual Presentation, CSRS42, June 22-24, Yellowknife, NWT, 2021.

[32] Science Toolbox exploitation platform (SNAP). https://step.esa.int/main/toolboxes/snap/, 2022 accessed July 2022.

[33] L. Dingle Robertson, A.M. Davidson, H. McNairn, M. Hosseini, S. Mitchell, D. De Abellleyra, S. Verón, M.H. Cosh, Synthetic Aperture Radar (SAR) image processing for operational space-based agriculture mapping, Int. J. Rem. Sens. 41 (18) (2020) 7112–7144, https://doi.org/10.1080/01431161.2020.1754494.

[34] X. Jiao, H. McNairn, B. Yekkehkhany, L. Dingle Robertson, S.O. Ihuoma, Integrating Sentinel-1 SAR and Sentinel-2 optical imagery with a crop structure dynamics model to track crop condition, Int. J. Rem. Sens. 43 (17) (2022) 6509–6537, https://doi.org/10.1080/01431161.2022.2142077.

[35] T.G. Farr, P.A. Rosen, E. Caro, R. Crippen, R. Duren, S. Hensley, M. Kobrick, M. Paller, E. Rodriguez, L. Roth, D. Seal eta, The shuttle radar topography mission, Rev. Geophys. 45 (2) (2007), https://doi.org/10.1029/2005RG000183.

[36] H. McNairn, C. Duguay, B. Brisco, T.J. Pultz, The effect of soil and crop residue characteristics on polarimetric radar response, Remote Sens. Environ. 80 (2002) 308–320, 10.1016/S0034-4257(01)00312-1.

[37] L. Dingle Robertson, H. McNairn, X. Jiao, C. McNairn, S.O. Ihuoma, Monitoring crops using compact polarimetry and the RADARSAT constellation mission, Can. J. Rem. Sens. 48 (6) (2022) 793–813, https://doi.org/10.1080/07038992.2022.2121271.

[38] S. Homayouni, H. McNairn, M. Hosseini, X. Jiao, J. Powers, Quad and compact multitemporal C-band PolSAR observations for crop characterization and monitoring, Int. J. Appl. Earth Obs. Geoinf. 74 (2019) 78–87, https://doi.org/10.1016/j.jag.2018.09.009.

[39] Government of Canada, Historical Climate Data, Climate, weather.gc.ca/, 2021 (accessed July 2022).

[40] U. Meier, A note on the power of Fisher's least significant difference procedure, Pharmaceut. Stat. 5 (4) (2006) 253–263, https://doi.org/10.1002/pst.210.

[41] S.O. Ihuoma, C.A. Madramootoo, Sensitivity of spectral vegetation indices for monitoring water stress in tomato plants, Comput. Electron. Agric. 163 (2019), https://doi.org/10.1016/j.compag.2019.104860.

[42] 'The Andersons', September 26, Corn Maturity and Drydown, andersonscanada.Com/2014/09/26/corn-Maturity-Drydown/, 2014 (accessed July 2022).

[43] K. Sarabandi, Y.-C. Lin, Simulation of interferometric SAR response for characterizing the scattering phase center statistics of forest canopies, IEEE Trans. Geosci. Rem. Sens. 38 (2000) 115–125, https://doi.org/10.1109/36.823906.